RSC Advances

PAPER

View Article Online
View Journal | View Issue

Cite this: *RSC Adv.*, 2016, **6**, 53669

C–H···Br–C *vs.* C–Br···Br–C *vs.* C–Br···N bonding in molecular self-assembly of pyridine-containing dyes†

Damir A. Safin, Maria G. Babashkina, Koen Robeyns and Yann Garcia*

Received 19th April 2016
Accepted 23rd May 2016

DOI: 10.1039/c6ra10094e

www.rsc.org/advances

We have studied a series of closely related *N*-(5-bromosalicylidene)-*x*-aminopyridine compounds (*x* = 2, **1**; 3, **2**; 4, **3**), obtained by condensation of 5-bromosalicylaldehyde with the corresponding aminopyridine. ^{1}H NMR spectroscopy in solution revealed a single structure, at least in $CDCl_3$. According to single crystal X-ray diffraction it was established that the crystal structures of **1–3** each are stabilized by a linear intramolecular hydrogen bond of the O–H···N type, formed between the hydroxyl hydrogen atom of the phenolic ring and the imine nitrogen atom. The dihalogen C–Br···Br–C and halogen C–Br···N(Py) interactions play a crucial role for the formation of supramolecular architectures in the structures of **2** and **3**, respectively. The overall geometry of each molecule in the structures of **1** and **2** was found to be almost planar, while a significantly twisted structure was found for **3**. Hirshfeld surface analysis showed that the structures of all compounds are mainly characterized by H···X contacts as well as by a remarkable contribution from C···C and C···N contacts which is clearly observed for **1** and **2**. Diffuse reflectance spectra of **1–3** each exhibit a mixture of enol, *cis*-keto and *trans*-keto forms. A major contribution of the *trans*-keto form is found for **1** whereas a moderate fraction is detected for **2**, and only traces of the *trans*-keto form were observed for **3**. Contrary to expectations based on dihedral angle Φ considerations, **1** exhibits negative photochromism, although it was expected to be only thermochromic. Both **2** and **3** are not photochromic, whereas **3** was expected to be photochromic ($\Phi > 25°$). Highly favoured C···C, C···N and O···Br intermolecular contacts as well as the absence of Br···Br dihalogen interactions in the structure of **1**, are presumably mainly responsible for the photochromic behaviour. Furthermore, significantly impoverished H···C and H···N contacts further support the observed negative photochromism of **1**.

Introduction

Crystal engineering[1] is a key strategy for the creation and design of new materials with desirable structures and properties, which depend on intermolecular interactions. Understanding of intermolecular interactions and packing in crystals is of the utmost importance for the fine tuning of a number of useful properties. Noncovalent interactions are considered as the most effective tool for the creation of molecular aggregates and assemblies.[1,2] Among these interactions, hydrogen bonds and π···π stacking are the most frequently used and legitimately take front rank due to their ability for rational design.[3]

On the other hand, short halogen atom contacts in crystals have grown to one of the most interesting noncovalent interactions for constructing supramolecular assemblies.[4] These interactions include halogen···halogen (X···X) and halogen···heteroatom (X···B) interactions. An IUPAC recommendation defining these interactions as halogen bonds was issued in 2013 and states that "*A halogen bond occurs when there is evidence of a net attractive interaction between an electrophilic region associated with a halogen atom in a molecular entity and a nucleophilic region in another, or the same, molecular entity*."[5] This definition highlights the qualitative analogy between halogen bonding and hydrogen bonding.

More than 50 years ago, Sakurai *et al.* noted that R–X···X–R contacts occur in two preferential geometries.[6] Much later, G. R. Desiraju and R. Parthasarathy classified these geometries as type I (symmetrical interactions where $\theta_1 = \theta_2$) and type II (bent interactions where $\theta_1 \approx 180°$ and $\theta_2 \approx 90°$) (Chart 1).[7] This classification is still valid nowadays. There is a clear geometric and chemical distinction between type I and type II X···X interactions. Type I interactions which are geometry-based contacts that arise from close-packing requirements, are found for all halogens, but are however not halogen bonds according to the IUPAC definition. Type II interactions arise from the pairing between the electrophilic area on one halogen

Institute of Condensed Matter and Nanosciences, Molecules, Solids and Reactivity (IMCN/MOST), Université Catholique de Louvain, Place L. Pasteur 1, 1348 Louvain-la-Neuve, Belgium. E-mail: yann.garcia@uclouvain.be; Fax: +32 1047 2330; Tel: +32 1047 2831

† Electronic supplementary information (ESI) available: Fig. S1–S3. CCDC 1470798 and 1470799. For ESI and crystallographic data in CIF or other electronic format see DOI: 10.1039/c6ra10094e

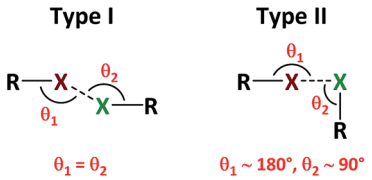

Chart 1 Structural scheme for type I and type II halogen···halogen short contacts.

atom and the electrophilic area on the other atom and are true halogen bonds.[8] Type II contacts are most favoured in iodinated derivatives, much less in brominated derivatives, and the least in chlorinated derivatives.[8b]

Halogen bonds, being selective and directional with their energy comparable to that of hydrogen bonds,[9] have extensively been used for designing molecular systems of desired properties,[10] such as molecular conductors, optoelectronic materials[11] and other functional materials.[12]

N-Salicylidene aniline derivatives (Scheme 1), as well as their *N*-heterocyclic analogues, dominate over other classes of molecules, exhibiting thermo- and photochromism in the crystalline state.[13] This is explained by both their colour panel and accessible forms (Scheme 1) as well as ease of synthesis, thanks to Schiff base condensation.[14] Another advantage of *N*-salicylidene aniline derivatives, making them attractive from a synthetic point of view, is the possibility to be included into various matrices to form hybrid materials,[15] and blends.[16]

The solid state thermochromic properties of *N*-salicylidene aniline derivatives were firstly considered to result from the planarity of the molecule and the formation of a "close-packed crystal structure" (dihedral angle between the aromatic rings $\Phi < 25°$), whereas photochromic behaviour is caused by the significant rotation of aromatic rings and the formation of an "open structure" ($\Phi > 25°$).[14] Thermo- and photochromic properties were even stated over the years to be mutually exclusive.[14b] A number of contradicting reports showing both thermo- and photochromic properties, have however been recently disclosed.[15b,17] All these newly obtained examples demonstrated that it is not possible to explain thermo- and photochromism of *N*-salicylidene aniline derivatives solely based on their crystal structures, but energy differences between ground and excited states need also to be considered.[15b] Furthermore, a complete and detailed crystal structure knowledge, including Φ, crystal packing and the available free space around the switching unit in addition to the flexibility of the nearby environment, is requested.[17f] All this is obviously dictated by a diversity of non-covalent intermolecular interactions responsible for the overall crystal packing of molecules.[18]

In continuation of our comprehensive studies of *N*-salicylidene aniline derivatives and with the aim to understand their structural features, which influence on their optical properties, we have directed our attention to a series of three closely related *N*-(5-bromosalicylidene)-*x*-aminopyridines (x = 2, **1**; 3, **2**; 4, **3**). Although both crystal structure and thermochromic properties of **1** were described,[19] it is also discussed herein for a better comparison with the two other compounds.

Due to the fact that the structures of molecules **1–3** could be efficiently stabilized by hydrogen bonding and halogen interactions, it was interesting to study the contribution and influence of intermolecular interactions in their crystal structures. Towards this aim, Hirshfeld surface analysis[20] and associated 2D fingerprint plots,[21] obtained using the CrystalExplorer 3.1 software,[22] as well as the enrichment ratios,[23] derived as the decomposition of the crystal contact surface between pairs of interacting chemical species, have been performed for the listed compounds.

Results and discussion

Compounds **1–3** were synthesized by reacting 5-bromosalicylaldehyde with the corresponding aminopyridine in ethanol (Scheme 2). The as-synthesized molecules form orange or yellow plate-like crystals, which are soluble in most polar solvents and are insoluble in *n*-hexane and diethylether.

^{1}H NMR spectra of **1–3** in $CDCl_3$ each reveal a single set of signals, which testifies to the presence of a single structure in solution. The signals for the benzene protons were found as two

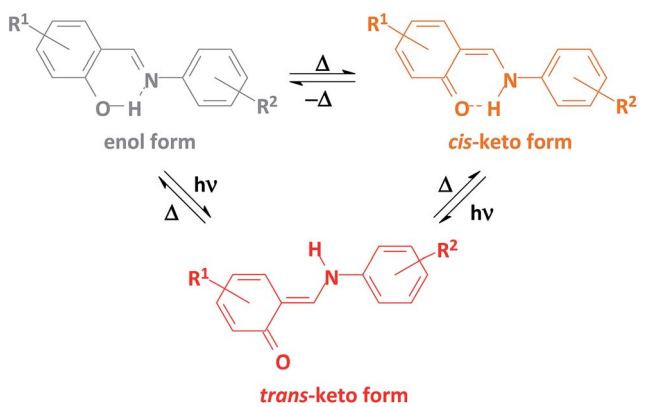

Scheme 1

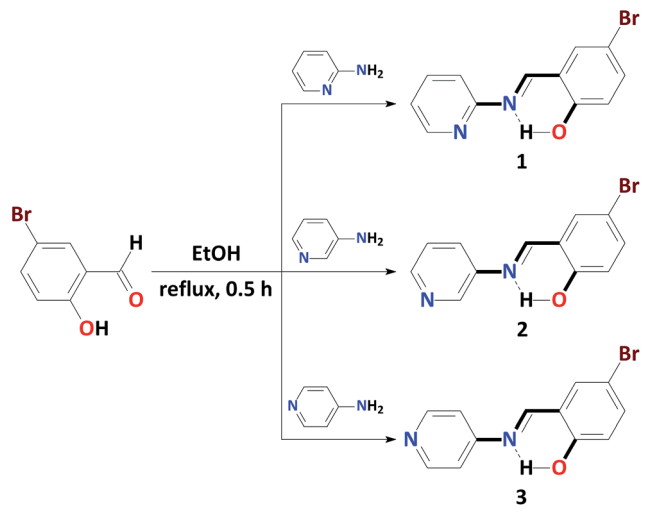

Scheme 2

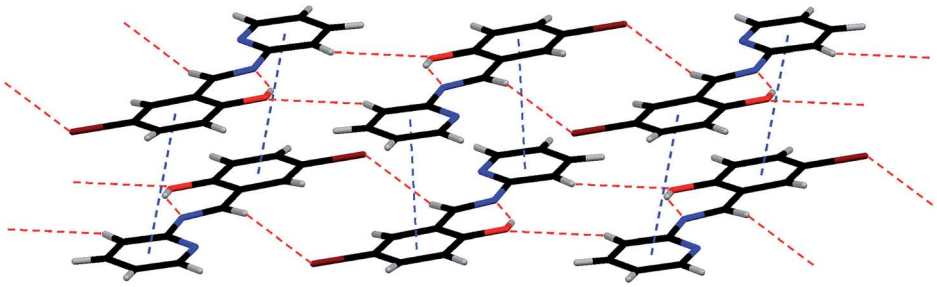

Fig. 1 View on the C–H···O–H and C–H···Br–C hydrogen bonded 1D polymeric chains, linked through π(Py)···π(C_6H_3) stacking interactions, in the structure of **1**. Colour code: C = black, H = light grey, N = blue, O = red, Br = brown.

doublets at 6.92–6.95 and 7.52–7.59 ppm and one doublet of doublets at 7.46–7.50 ppm, respectively. Two singlet signals for the arylCHN and OH protons were observed at 8.54–9.37 and 12.57–13.48 ppm, respectively. The pyridine protons in the spectra were observed as a number of signals with different multiplicities at 7.12–8.66 ppm.

The crystal structures of **2** and **3** were elucidated by single crystal X-ray diffraction. Crystals of **1** correspond to the reported structure.[19] Their structural parameters were extracted and used herein to compare with those of **2** and **3**. Compounds **1** and **2** each crystallize in the monoclinic space groups $P2_1/n$, while the structure of **3** was refined in the orthorhombic space group $Pca2_1$.

Molecules in all the three structures were found in the enolimine form (Fig. 1–3). The bond lengths of C–O, with respect to the moieties marked in bold in Scheme 2, are about 1.35 Å and those of C–C are about 1.45 Å (Table 1), which indicate single bonds, whereas a double bond of about 1.28 Å is revealed for C=N (Table 1). The bond angles C–C=N and C–N=C of 119.2(4)–122.9(4)° indicate an sp^2-hybridization of both carbon and nitrogen atoms of the imine fragment, further supporting the enolimine form (Table 1). The crucial difference between the structures **1–3** consists in the dihedral angle *Φ* between benzene and pyridine rings. While in **1** and **2**, the two rings are at about 5.5°, the dihedral angle is remarkably larger in **3** and of about 42.4° (Table 1).

All molecules are stabilized by a typical intramolecular hydrogen bond between the hydroxyl hydrogen and the imine nitrogen atoms (Fig. 1–3 and Table 2). The crystal structure of **1**

Table 1 Selected bond lengths (Å) and angles (°) for **1–3**[a]

	1	**2**	**3**
Bond lengths			
C=N	1.281(6)	1.268(4)	1.281(5)
C–C	1.467(7)	1.453(4)	1.433(6)
C–O	1.346(6)	1.350(4)	1.358(5)
C–N	1.424(6)	1.424(4)	1.416(5)
Bond angles			
C–C=N	121.6(4)	122.5(2)	122.9(4)
C–N=C	119.2(4)	121.3(2)	120.8(3)
Torsion angles			
C–C=N–C	−179.2(4)	179.0(3)	173.1(3)
Dihedral angles (*Φ*)			
C_6H_3–Py	5.2(3)	5.58(15)	42.44(19)

[a] Values with respect to the moieties marked by bold in Scheme 2.

Table 2 Hydrogen and halogen bond lengths (Å) and angles (°) for **1–3**

	D–X···A	*d*(D–X)	*d*(X···A)	*d*(D···A)	∠(DXA)
1[a]	O(1)–H(1)···N(1)	0.74(5)	1.95(5)	2.619(5)	151(4)
	C(10)–H(7)···O(1)$^{\#1}$	0.98(4)	2.54(4)	3.383(6)	144(4)
	C(7)–H(5)···Br(1)$^{\#2}$	1.08(5)	2.93(4)	3.911	151(3)
2[b]	O(8)–H(8)···N(10)	0.82	1.91	2.632(3)	147
	C(2)–Br(1)···Br(1)$^{\#1}$	1.898(3)	3.5747(6)	5.029	131.05(9)
3[c]	O(8)–H(8)···N(10)	0.82	1.87	2.602(5)	148
	C(2)–Br(1)···N(14)$^{\#1}$	1.901(4)	3.150(4)	5.036	170.82(13)

[a] Symmetry transformations used to generate equivalent atoms: #1 −1 − *x*, −*y*, −2 − *z*; #2 −*x*, −*y*, −*z*. [b] Symmetry transformations used to generate equivalent atoms: #1 2 − *x*, 1 − *y*, −*z*. [c] Symmetry transformations used to generate equivalent atoms: #1 5/2 − *x*, *y*, 1/2 + *z*.

Table 3 π···π interaction distances (Å) and angles (°) for **1** and **2**[a]

	Cg(*I*)	Cg(*J*)	*d*[Cg(*I*)–Cg(*J*)]	*α*	*β*	*γ*	Slippage
1[b]	Cg(1)	Cg(2)$^{\#1}$	3.805(3)	5.2(3)	22.3	21.4	1.443
	Cg(2)	Cg(1)$^{\#1}$	3.805(3)	5.2(3)	21.4	22.3	1.389
	Cg(1)	Cg(2)$^{\#2}$	4.478(3)	5.2(3)	38.7	39.4	2.801
	Cg(2)	Cg(1)$^{\#2}$	4.477(3)	5.2(3)	39.4	38.7	2.842
2[c]	Cg(1)	Cg(1)$^{\#1}$	4.5102(19)	0.03(16)	39.8	39.8	2.890
	Cg(1)	Cg(1)$^{\#2}$	4.5102(19)	0.03(16)	39.8	39.8	2.890
	Cg(2)	Cg(2)$^{\#1}$	4.5102(17)	0.00(14)	41.2	41.2	2.971
	Cg(2)	Cg(2)$^{\#2}$	4.5104(17)	0.00(14)	41.2	41.2	2.972

[a] Cg(*I*)–Cg(*J*): distance between ring centroids; *α*: dihedral angle between planes Cg(*I*) and Cg(*J*); *β*: angle Cg(*I*) → Cg(*J*) vector and normal to plane *I*; *γ*: angle Cg(*I*) → Cg(*J*) vector and normal to plane *J*; slippage: distance between Cg(*I*) and perpendicular projection of Cg(*J*) on ring *I*. [b] Symmetry transformations used to generate equivalent atoms: #1 −1 − *x*, −*y*, −1 − *z*; #1 −*x*, −*y*, −1 − *z*. Cg(1): N(2)–C(8)–C(9)–C(10)–C(11)–C(12); Cg(2): C(1)–C(2)–C(3)–C(4)–C(5)–C(6). [c] Symmetry transformations used to generate equivalent atoms: #1 −1 + *x*, *y*, *z*; #1 1 + *x*, *y*, *z*. Cg(1): N(15)–C(14)–C(13)–C(12)–C(11)–C(16); Cg(2): C(2)–C(3)–C(4)–C(5)–C(6)–C(7).

contains linear intermolecular hydrogen bonds of the C–H···O–H type, formed between the hydroxyl oxygen atom and the pyridine 3-H atom (Table 2) with the formation of $R^2_2(16)$ centrosymmetric dimers (Fig. 1). These dimers are linked to each other, yielding 1D ribbons, through the C–H···Br–C hydrogen bonds formed between the bromine atom and the imine hydrogen atom with the formation of $R^2_2(12)$ centrosymmetric cycles (Fig. 1 and Table 2). These ribbons are further linked in 2D sheets through π···π stacking interactions between the pyridine and benzene rings (Fig. 1 and Table 3).

In the crystal structure of **2**, centrosymmetric dimers are also formed but linked through C–Br···Br–C intermolecular type I dihalogen interactions (Fig. 2 and Table 2). The Br···Br distances 3.5747(6) Å are notably shorter than the sum of two van der Waals radii for bromine (1.85 Å).[24] This proves the key relevance of the Br···Br halogen interaction in driving the self-assembly of **2** to give the dimeric architecture (Fig. 2). These dimers are further linked into 1D ribbons due to π···π stacking interactions between the same type of aromatic rings (Fig. 2 and Table 3).

In general, π···π stacking interactions in the structures of **1** and **2** are formed between almost perfectly flat adjacent molecules, situated on top of each other, with a slippage distance of about one-half or one benzene ring diameter (Table 3). "Head-to-tail" or "head-to-head" stackings are adopted in **1** and **2**, respectively (Fig. 1 and 2). Distances between the least squares planes formed by adjacent parallel molecules is about 3.40 Å and 3.54 Å in the structure of **1** and 3.42 Å in the structure of **2**.

Thanks to the C–Br···N type I intermolecular halogen interactions, formed between bromine and pyridine nitrogen atoms, molecules of **3** are linked into 1D polymeric chains (Fig. 3 and Table 2). The Br···N distances are 3.150(4) Å and are substantially shorter than the sum of the van der Waals radii for nitrogen (1.55 Å) and bromine (1.85 Å).[24] The shortening of the Br···N van der Waals distance is about 8% and also proves the key relevance of the Br···N halogen bonding in driving the self-assembly of **3** to give the 1D polymeric chain architecture (Fig. 3). These chains are further linked into 2D sheets through C–H···π interactions (Fig. 3 and Table 4).

According to the Hirshfeld surface analysis, for the molecule of **1**, intermolecular H···H contacts, comprising 35.6% of the total number of contacts, are major contributors to the crystal packing (Table 5). A proportion of the same contacts notably decreases in the structure of **2** and further decreases in the structure of **3**, comprising 29.9% and 26.1%, respectively (Table 5). The shortest H···H contacts are shown in the fingerprint plots of **1–3** at $d_e + d_i \approx$ 2.2–2.4 Å (Fig. S1–S3 in the ESI†). Furthermore, a subtle feature is evident in the fingerprint plot of **1**. There is a splitting of the short H···H fingerprint. This splitting occurs when the shortest contact is between three

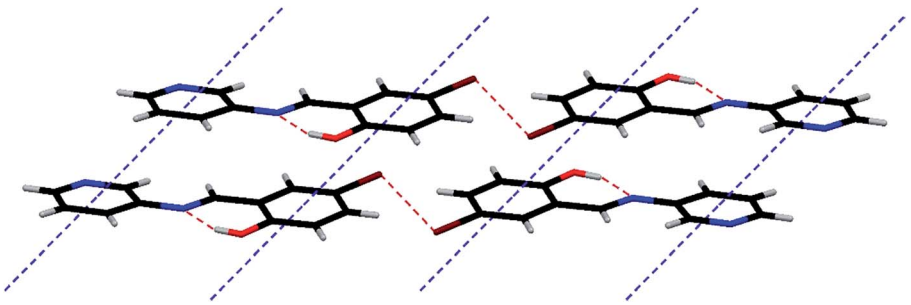

Fig. 2 View on the C–Br···Br–C dihalogen bonded dimers, linked through π(Py)···π(Py) and π(C_6H_3)···π(C_6H_3) stacking interactions, in the structure of **2**. Colour code: C = black, H = light grey, N = blue, O = red, Br = brown.

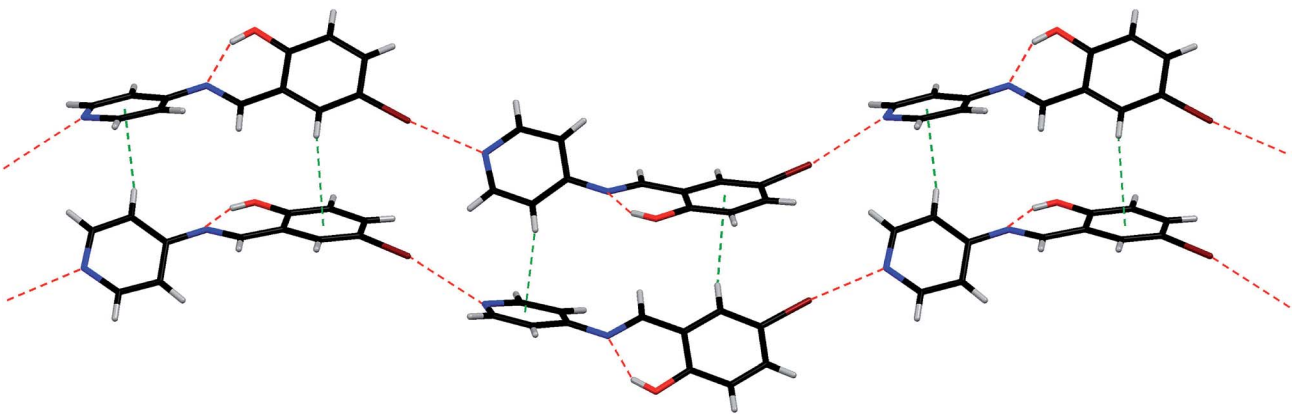

Fig. 3 View on the C–Br···N halogen bonded 1D polymeric chains, linked through C–H(Py)···π(Py) and C–H(C_6H_3)···π(C_6H_3) interactions, in the structure of **3**. Colour code: C = black, H = light grey, N = blue, O = red, Br = brown.

Table 4 C–H···π interaction distances (Å) and angles (°) for **3**[a]

C–H	Cg(*J*)	*d*[H···Cg(*J*)]	*d*[C···Cg(*J*)]	∠[C–H···Cg(*J*)]	H-Perp
C(7)–H(7)	Cg(2)$^{\#1}$	2.98	3.616(4)	127	−2.95
C(12)–H(12)	Cg(1)$^{\#2}$	2.76	3.450(5)	132	−2.76

[a] H-Perp: perpendicular distance of H to ring plane *J*. Symmetry transformations used to generate equivalent atoms: #1 1/2 + *x*, 1 − *y*, *z*; #2 −1/2 + *x*, 1 − *y*, *z*. Cg(1): N(14)–C(13)–C(12)–C(11)–C(16)–C(15); Cg(2): C(2)–C(3)–C(4)–C(5)–C(6)–C(7).

atoms, rather than for a direct two-atom contact.[20] The structures of **1–3** are also dominated by H···C and H···Br contacts. While the latter contacts occupy a similar proportion of the molecular surfaces of **1–3** (17.0–19.5%), the former contacts reveal an opposite trend, compared to the H···H contacts, and comprise 13.8%, 17.8% and 29.5%, of the total Hirshfeld surface areas, respectively. Notably, a proportion of H···C contacts is the most dominant one in the structure of **3**. The H···C contacts in the fingerprint plot of **3** are shown in the form of clearly pronounced "wings" (Fig. S3 in the ESI†), with the shortest $d_e + d_i \approx 2.8$ Å. These contacts are recognized as characteristic of C–H···π nature,[20] and correspond to the abovementioned interactions, which link 1D polymeric chains into 2D sheets in the structure of **3** (Fig. 3 and Table 4). The H···Br contacts in the fingerprint plots of **1–3** are shown in the form of a pair of broad "horns" with the shortest $d_e + d_i \approx 2.9$–3.1 Å

Table 5 2D fingerprint plots, Hirshfeld contact surfaces and derived "random contacts" and "enrichment ratios" for **1–3**

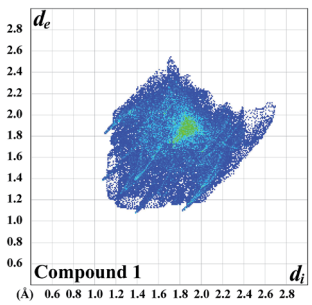

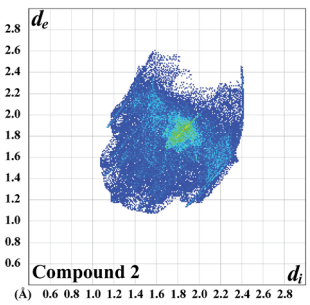

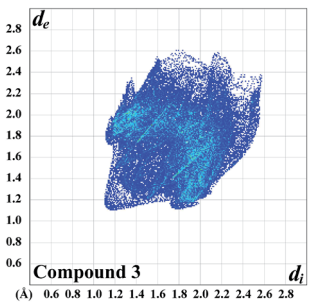

	H	C	N	O	Br	H	C	N	O	Br	H	C	N	O	Br
Contacts (*C*, %)[a]															
H	35.6	—	—	—	—	29.9	—	—	—	—	26.1	—	—	—	—
C	13.8	10.7	—	—	—	17.8	8.2	—	—	—	29.5	2.0	—	—	—
N	4.3	3.8	1.0	—	—	7.4	5.1	0.8	—	—	10.4	0.0	0.0	—	—
O	8.4	0.0	0.2	0.0	—	8.6	0.2	0.2	0.0	—	6.1	3.2	0.1	0.0	—
Br	19.3	0.6	1.4	0.9	0.0	19.5	0.7	0.0	0.4	1.3	17.0	1.6	3.5	0.0	0.3
Surface (*S*, %)															
	58.5	19.8	5.9	4.8	11.1	56.6	20.1	7.2	4.7	11.6	57.6	19.2	7.0	4.7	11.4
Random contacts (*R*, %)															
H	34.2	—	—	—	—	32.0	—	—	—	—	33.2	—	—	—	—
C	23.2	3.9	—	—	—	22.8	4.0	—	—	—	22.1	3.7	—	—	—
N	6.9	2.3	0.3	—	—	8.2	2.9	0.5	—	—	8.1	2.7	0.5	—	—
O	5.6	1.9	0.6	0.2	—	5.3	1.9	0.7	0.2	—	5.4	1.8	0.7	0.2	—
Br	13.0	4.4	1.3	1.0	1.2	13.1	4.7	1.7	1.1	1.3	13.1	4.4	1.6	1.1	1.3
Enrichment (*E*)[b]															
H	1.04	—	—	—	—	0.93	—	—	—	—	0.79	—	—	—	—
C	0.59	2.74	—	—	—	0.78	2.05	—	—	—	1.33	0.54	—	—	—
N	0.62	1.65	—	—	—	0.90	1.76	—	—	—	1.28	0.00	—	—	—
O	1.50	0.00	—	—	—	1.62	0.11	—	—	—	1.13	1.78	—	—	—
Br	1.48	0.14	1.08	0.90	0.00	1.49	0.15	0.00	0.36	1.00	1.30	0.36	2.19	0.00	0.23

[a] Values are obtained from CrystalExplorer 3.1.[22] [b] The enrichment ratios were not computed when the "random contacts" were lower than 0.9%, as they are not meaningful.[23]

(Fig. S1–S3 in the ESI†). These shortest H···Br contacts in the structure of **1** correspond to the above mentioned C–H···Br–C hydrogen bonds responsible for the formation of 1D ribbons from $R^2_2(16)$ centrosymmetric dimers (Fig. 1 and Table 2).

Further contributions into molecular surfaces of **1–3** arise from H···N and H···O contacts (Table 5). While the latter contacts occupy a similar proportion of the total Hirshfeld surface in all the structures (6.1–8.6%), the fraction of the former contacts proportionally increases from **1** (4.3%) to **2** (7.4%) to **3** (10.4%). The H···O contacts in the fingerprint plot of **1** are shown as a pair of relatively sharp spikes with the shortest $d_e + d_i \approx 2.5$ Å (Fig. S1 in the ESI†), and correspond to the above mentioned C–H···O–H hydrogen bonds responsible for the formation of $R^2_2(16)$ centrosymmetric dimers (Fig. 1 and Table 2).

The molecular surface of **1** and **2** are further characterized by C···C and C···N contacts, comprising 8.2–10.7% and 3.8–5.1%, respectively (Table 5). While the former contacts are significantly impoverished (2.0%) in the structure of **3**, the latter contacts are completely absent. The C···C contacts are shown on the fingerprint plots of **1** and **2** as the characteristic pale blue/green, mixed with yellow points, area on the diagonal at $d_e = d_i \approx 1.7$–2.0 Å (Fig. S1 and S2 in the ESI†), and attributed to the formation of the above mentioned strong π···π stacking interactions (Fig. 1, 2 and Table 3). The C···N contacts are shown on the fingerprint plots of **1** and **2** as the characteristic symmetric area on the same diagonal at $d_e = d_i \approx 1.8$–2.0 Å (Fig. S1 and S2 in the ESI†), and also correspond to strong π···π stacking interactions (Fig. 1, 2 and Table 3). It should be noted, that the difference in the nature of π···π stacking interactions in the structures of **1** and **2** is clearly reflected in a higher proportion of C···C contacts and a lower proportion of C···N contacts in the former structure compared with those in the latter one (Table 5). Notably, Br···Br and N···Br contacts, responsible for the halogen interactions in the structures **2** and **3**, respectively, comprise 1.3% and 3.5% of the total Hirshfeld surface areas. The Br···Br contacts are shown on the fingerprint plot of **2** as the pale blue/green, mixed with yellow points, sharp spike on the diagonal at $d_e = d_i \approx 1.8$–2.2 Å (Fig. S2 in the ESI†). The N···Br contacts in the fingerprint plot of **3** are shown as a pair of sharp spikes with the shortest $d_e + d_i \approx 3.1$ Å (Fig. S3 in the ESI†). While the Br···Br contacts are completely absent, a minor proportion of the N···Br contacts (1.4%) were also found on the molecular surface of **1** (Table 5). However, these contacts are shown on the fingerprint plot of **1** as a pair of small spikes with the shortest $d_e + d_i \approx 3.6$ Å (Fig. S1 in the ESI†), which is significantly longer than the sum of van der Waals radii for nitrogen (1.55 Å) and bromine (1.85 Å).[24]

It is worth to mention, that the molecular surface of **3** is also populated by C···O and C···Br contacts, comprising 3.2% and 1.6%, respectively. Close inspection of other intermolecular contacts in the structures of **1** and **2** also revealed a negligible proportion of C···Br (0.6–0.7%), N···N (0.8–1.1%), N···O (0.2%) and O···Br (0.4–0.9%), as well as C···O (0.2%) in **2**, contacts (Table 5, Fig. S1 and S2 in the ESI†). The molecular surface of **3** also exhibits a negligible proportion of N···O (0.1%) and Br···Br (0.3%) contacts.

The enrichment ratios (E)[23] of the intermolecular contacts for **1–3** were also determined to study the propensity of two chemical species to be in contact. The enrichment ratio, derived from the Hirshfeld surface analysis, is defined as the ratio between the proportion of actual contacts in the crystal and the theoretical proportion of random contacts. E is larger than unity for pair of elements with a higher propensity to form contacts, while pairs which tend to avoid contacts yield a E value lower than unity.

H···H contacts are favoured in the structure of **1** since the enrichment ratio $E_{HH} = 1.04$ and generate a majority (35.6%) of the interaction surface (Table 5). Contrarily, H···H contacts are less favoured in the structure of **2** ($E_{HH} = 0.93$) and even much less favoured in the structure of **3** ($E_{HH} = 0.79$). This is explained by a significantly lower proportion (29.9% and 26.1%, respectively) of the H···H contacts of the total Hirshfeld surface area in **2** and **3**, although their structures contain almost the same amount of random contacts R_{HH} as well as each are characterized by a high S_H proportion as in the structure of **1** (Table 5). The opposite trend is observed for H···C and H···N contacts, which show an increased propensity to form ($E_{HC} = 1.33$, $E_{HN} = 1.28$) in the structure of **3**, and only slightly favoured ($E_{HC} = 0.78$, $E_{HN} = 0.90$) in **2**, and impoverished ($E_{HC} = 0.59$, $E_{HN} = 0.62$) in **1**. This is explained by comparable higher amounts of H···C and H···N contacts of the total Hirshfeld surface area compared to those in **2** and **1**, despite both structures are characterised by almost the same values of the S_H, S_C and S_N proportions, and random contacts R_{HC} and R_{HN} (Table 5). The E_{HO} and E_{HBr} values are larger than unity (1.13–1.62) for all molecules, indicating that H···O and H···Br contacts have an increased propensity to form, with extremely close random contacts ($R_{HO} = 5.3$–5.6, $R_{HBr} = 13.0$–13.1).

Remarkably, the structure of **2** is further characterized by highly favoured C···C contacts ($E_{CC} = 2.05$), while the same contacts in the structure of **1** are even more favoured ($E_{CC} = 2.74$). This is due to a negligible amount of random contacts R_{CC} (3.9–4.0%). Despite the molecule of **3** is characterised by almost the same proportion of random contacts R_{CC} (3.7%), the C···C contacts are significantly impoverished ($E_{CC} = 0.54$), which is explained by a negligible proportion of these contacts (2.0%) on the total Hirshfeld surface of **3**. Furthermore, the C···N contacts are highly favoured in the structures of **1** and **2** since the corresponding enrichment ratios E_{CN} are higher than unity (1.65 and 1.76, respectively). Interestingly, while the E_{NBr} value is slightly higher than unity for the structure of **1**, the same contacts are much more favoured in the structure of **3** ($E_{NBr} = 2.19$), which is explained by a significantly higher amount of N···Br contacts on the molecular surface of **3** compared to that of **1** (Table 5). Moreover, a similar trend can be applied to explain highly favoured C···O contacts in the structure of **3** ($E_{CO} = 1.78$), while the same contacts are very impoverished in the structure of **2** ($E_{CO} = 0.11$) and completely absent in **1** (Table 5). The opposite trend is found for the O···Br contacts. In particular, while these contacts are almost favoured in the structure of **1** since the enrichment ratio E_{OBr} is close to unity (0.90), the same contacts are significantly impoverished (0.36) in **2** and completely absent in **3**. This is obviously due to a remarkable

difference in the proportion of the O···Br contacts on the molecular surfaces of **1–3** (0.0%, 0.4% and 0.9% respectively), while very similar values for S_O (4.7–4.8%), S_{Br} (11.1–11.6%) and R_{OBr} (1.0–1.1%) were found (Table 5). Finally, the C···Br (E_{CO} = 0.14–0.36) contacts in all the structures, as well as Br···Br contacts in **3** (E_{BrBr} = 0.23), are significantly impoverished, while the structure of **2** is enriched by Br···Br contacts as evidenced from the enrichment ratio E_{BrBr} equal to unity.

Compounds **1–3** were analyzed by diffuse reflectance spectroscopy (DRS) as pure solid powders to avoid matrix and environment effects that are known to intensively modify the optical properties of *N*-salicylidene aniline derivatives.[15b,c]

Diffuse reflectance spectra of **1–3**, for which a Kubelka–Munk (KM) treatment was applied, each exhibit three band regions: a broad band range in the UV region, corresponding to the enol form, a second range in the visible region from about 375 to 450 nm, originating from the *cis*-keto form, and a third range above 450 nm, originating from the *trans*-keto form (Fig. 4). A major contribution of the *trans*-keto form is found for **1** whereas a moderate fraction is detected for **2**, and only traces of the *trans*-keto form were observed for **3** (Fig. 4). All compounds were also analyzed by DRS upon irradiation at selected wavelengths (λ = 254, 365, 450 and 546 nm) in order to photo-address enol and keto forms.

Contrary to expectations based on dihedral angle Φ considerations, **1** is photochromic upon irradiation at λ = 546 nm (Fig. 4), although it was expected to be only thermochromic (Φ < 25°).[19] A similar negative photochromism was observed for *N*-(3,5-dichlorosalicylidene)-1-aminopyrene[25] and 15-crown-5 ether-containing *N*-salicylidene aniline.[26] Furthermore, both **2** and **3** are not photochromic regardless of the irradiation wavelength and time, whereas **3** was expected to be also photochromic (Φ > 25°).

Solid state fluorimetric studies of **1–3** crystals were undertaken to examine energy levels responsible for the photoswitchable optical properties. The emission spectra at λ_{exc} = 400 nm, which corresponds to the band of the *cis*-keto form in the diffuse reflectance spectra (Fig. 4), are shown in Fig. 5. Two intense bands centred at about 570 and 595 nm are observed for **3** and, most likely, for **2** with a single broad band at 570 nm, while only one relatively narrow band centred at 585 nm is observed in the spectrum of **1**. The fluorescence has been assigned to the emission from the *cis*-keto form, which is produced through proton transfer in the excited-state of the enol form. Therefore, an anomalously large Stokes shift is observed. The longer wavelength band originates from the emission of the more stable and relaxed conformation of the *cis*-keto form and the band at the shorter wavelength is due to the emission from the less stable planar conformation.[27] A third weak emission band is also noted at about 650 nm for **1–3** (Fig. 5), which is much more pronounced in the spectrum of **1**, in the region of the *trans*-keto form, as deduced from diffuse reflectance data (Fig. 4).

Excitation spectra of **1–3** recorded at λ_{em} = 620 nm each reveal two high-energy contributions centred at about 420 and 500 nm (Fig. 5), with the latter band being significantly less pronounced in the spectrum of **1**. These bands are assigned to the emission of two different conformers of the *cis*-keto* forms in the excited state. The low-energy band is due to the emission from the more stable and relaxed conformation, whereas the high-energy band is due to the emission from the less stable planar conformation.[27] The spectra of **1** and **2** also exhibit a third low-energy band, which is barely observed in the spectrum of **2**, centred at about 590 nm (Fig. 5). This band can be assigned to the absorption of the *trans*-keto form by comparison with diffuse reflectance spectroscopy (Fig. 4). The emission at about 650 nm can thus be assigned to the radiative relaxation of the *trans*-keto* form, which can be formed through the absorption of enol, *cis*-keto and *trans*-keto forms in their ground state.[28]

Optical properties of *N*-salicylidene aniline derivatives were first systematically studied by Cohen and Schmidt in the sixties of the past century,[29] and are still under debate being in the limelight of many researches.[30] UV irradiation of the enol form leads to the formation of the excited enol* form (Fig. 6). This species can fluoresce in the visible region in some rare cases,[15b] or complete a fast tautomerization to the excited *cis*-keto* form.

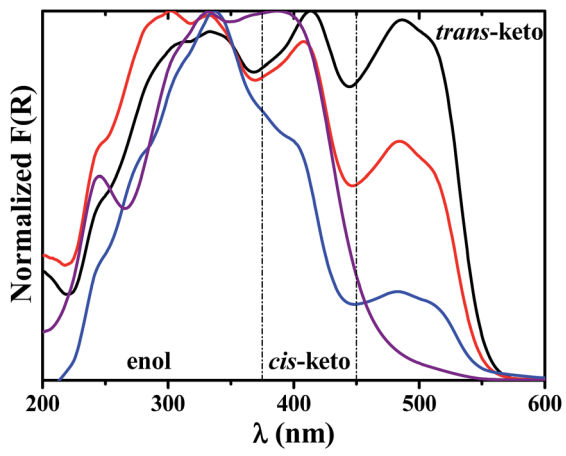

Fig. 4 Normalized KM spectra of **1** before (black) and after (red) irradiation at λ_{exc} = 546 nm for 30 min, **2** (blue) and **3** (purple) at 23 °C.

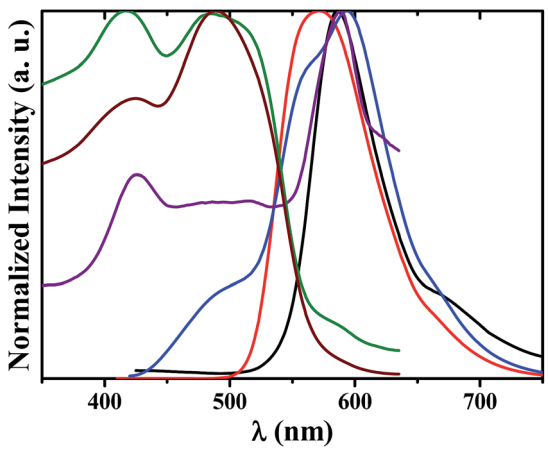

Fig. 5 Normalized solid-state emission and excitation spectra of **1** (Em – black, Ex – purple), **2** (Em – red, Ex – olive) and **3** (Em – blue, Ex – brown) at 23 °C (λ_{exc} = 400 nm, λ_{em} = 620 nm).

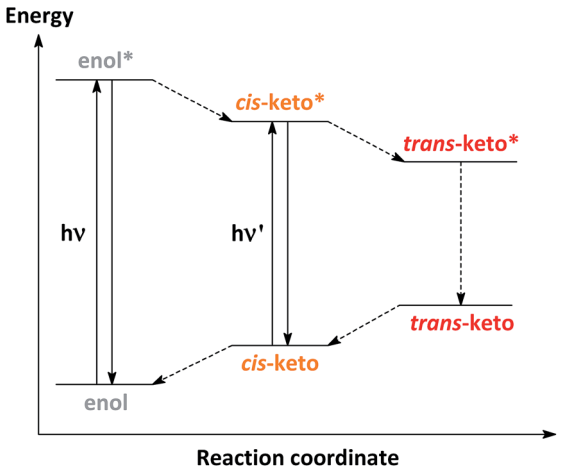

Fig. 6 Photochemical process leading to the formation of the *trans*-keto form from the enol form for *N*-salicylideneaniline aniline derivatives. The solid arrows indicate absorption phenomena or emission relaxation and the dotted arrows represent non-radiative relaxation.

The *cis*-keto* to *cis*-keto relaxation is mainly radiative and is always detected by fluorescence spectroscopy. The *cis*-keto* form can also undergo photoisomerization to produce the excited *trans*-keto* form, which is described to be non-fluorescent. It is assumed that the *trans*-keto* to *trans*-keto relaxation is mostly non-radiative. Back reaction from *trans*-keto to *cis*-keto and enol forms is either thermally or photochemically induced. The latter reaction, namely negative photochromism in the present case, was observed for **1** (Fig. 4).

Among the reported structures, only **1** exhibits pronounced photochromic properties, although of negative nature. This is surprising since **1**, as well as **2**, were expected to be exclusively thermochromic, while **3** was expected exclusively photochromic based on the widely shared structural perceptions for *N*-salicylidene aniline derivatives.[14] Elucidated contradictions within **1–3**, most likely, can be explained by the fine combination of favoured and even highly favoured C···C, C···N and O···Br contacts as well as the absence of Br···Br dihalogen interactions (Table 5). Furthermore, significantly impoverished H···C and H···N contacts (Table 5) further support the observed negative photochromism of **1**. Moreover, these supramolecular factors can also influence on the energy differences between ground and excited states, which, in turn, can favour the formation of the keto form. Detailed theoretical studies which are in progress in our laboratory are required to check this latter hypothesis.

Conclusions

In summary, a series of three closely related *N*-(5-bromosalicylidene)-*x*-aminopyridine compounds **1–3** has been successfully prepared by the condensation reaction of 5-bromosalicylaldehyde with the corresponding aminopyridine. All the compounds were studied by means of ^{1}H NMR spectroscopy in solution, revealing the presence of a single structure at least in $CDCl_3$.

According to single crystal X-ray diffraction, it was established, that the crystal structures of **1–3** are stabilized by a linear intramolecular hydrogen bond of the O–H···N type, formed between the hydroxyl hydrogen atom of the phenolic ring and the imine nitrogen atom. In addition, the dihalogen C–Br···Br–C and halogen C–Br···N(Py) interactions play a crucial role for the formation of supramolecular architectures in the crystal structures of **2** and **3**, respectively. The overall geometry of each molecule in the structures of **1** and **2** was found to be almost planar, while a significantly twisted structure was established for **3**.

Hirshfeld surface analysis showed that the structures of all compounds are mainly characterized by H···X contacts as well as a remarkable contribution from C···C and C···N contacts which is clearly observed for **1** and **2**.

Diffuse reflectance spectra of **1–3** each reveal a mixture of the enol, *cis*-keto and *trans*-keto forms. A major contribution is found for **1** whereas a moderate fraction is detected for **2**, and only traces of the *trans*-keto form were observed for **3**. Contrary to expectations based on dihedral angle Φ considerations, **1** exhibits negative photochromism, although it was expected to only be thermochromic. Both **2** and **3** are not photochromic, whereas **3** was expected to be also photochromic ($\Phi > 25°$). We have postulated that highly favoured C···C, C···N and O···Br intermolecular contacts as well as the absence of Br···Br dihalogen interactions in the structure of **1**, are mainly responsible for the photochromic behaviour. Furthermore, significantly impoverished H···C and H···N contacts further support the observed negative photochromism of **1**. These pyridine containing dyes bear potential interest in iron(II) coordination chemistry since one could expect to get functional materials whose spin state could be modified by fine tuning of optical properties.[15b]

Experimental

Physical measurements

^{1}H NMR spectra in $CDCl_3$ were obtained on a Bruker AC 300 MHz spectrometer at 25 °C. Diffuse reflectance spectra were obtained with a Varian Cary 5E spectrometer using polytetrafluoroethylene (PTFE) as a reference. Spectra were measured on pure solids to avoid matrix effects. Eventual distortions in the Kubelka–Munk spectra that could result from the study of pure compounds have not been considered because no comparison with absorption spectra was necessary. Light irradiations were carried out with a LOT-ORIEL 200 W high-pressure mercury Arc lamp (LSN261). Elemental analyses were performed on a CHNS HEKAtech EuroEA 3000 analyzer.

Hirshfeld surface analysis

The Hirshfeld molecular surfaces[20] and their associated 2D fingerprint plots[21] were generated using the CrystalExplorer 3.1 software[22] on the basis of crystal structures. The d_{norm} (normalized contact distance) surface and the breakdown of the 2D fingerprint plots were used for decoding and quantifying the intermolecular interactions in the crystal lattice. The d_{norm} is a symmetric function of distances to the surface from the nuclei inside (d_i) and outside (d_e) the Hirshfeld surface, relative to

their respective van der Waals radii. 2D fingerprint plots were generated using d_i and d_e in the translated 0.4–3.0 Å range and including reciprocal contacts as a pair of coordinates in 2D histograms. A colour gradient in the fingerprint plots ranging from blue to red is used to visualize the proportional contribution of contact pairs in the global surface.

Enrichment ratio

The enrichment ratio (E)[23] of a pair of elements (X, Y) is the ratio between the proportion of actual contacts in the crystal and the theoretical proportion of random contacts. E is larger than unity for pairs of elements which have a high propensity to form contacts in crystals, while pairs which tend to avoid contacts with each other yield an E value lower than unity. E values are calculated from the percentage of contacts, which, in turn, are given by the CrystalExplorer 3.1 software,[21] between one type or two types of chemical elements in a crystal packing.

Synthesis of 1–3

A solution of 5-bromosalicylaldehyde (10 mmol, 2.010 g) dissolved in ethanol (20 mL) was added to a solution of 2-, 3- or 4-aminopyridine (10 mmol, 0.941 g) in the same solvent (20 mL). The mixture was stirred under reflux for 0.5 h. The resulting solution was allowed to cool to room temperature to give X-ray suitable crystals of **1–3**.

1. ^{1}H NMR: $\delta = 6.92$ (d, $^3J_{H,H} = 8.8$ Hz, 1H, 3-H, C_6H_3), 7.24 (t. d, $^3J_{H,H} = 7.8$ Hz, $^4J_{H,H} = 1.8$ Hz, 1H, 5-H, Py), 7.32 (d, $^3J_{H,H} = 7.9$ Hz, 1H, 3-H, Py), 7.46 (d. d, $^3J_{H,H} = 8.8$ Hz, $^4J_{H,H} = 2.3$ Hz, 1H, 4-H, C_6H_3), 7.59 (d, $^4J_{H,H} = 2.3$ Hz, 1H, 6-H, C_6H_3), 7.78 (t. d, $^3J_{H,H} = 7.9$ Hz, $^4J_{H,H} = 1.8$ Hz, 1H, 4-H, Py), 8.51 (d. d, $^3J_{H,H} = 4.7$ Hz, $^4J_{H,H} = 1.2$ Hz, 1H, 6-H, Py), 9.37 (s, 1H, arylCHN), 13.48 (s, 1H, OH) ppm. Calc. for $C_{12}H_9BrN_2O$ (277.12): C 52.01, H 3.27; N 10.11. Found: C 52.12, H 3.32, N 10.16.

2. ^{1}H NMR: $\delta = 6.93$ (d, $^3J_{H,H} = 8.8$ Hz, 1H, 3-H, C_6H_3), 7.37 (d. d, $^3J_{H,H} = 7.9$ Hz, $^4J_{H,H} = 3.2$ Hz, 1H, 5-H, Py), 7.47 (d. d, $^3J_{H,H} = 8.8$ Hz, $^4J_{H,H} = 2.1$ Hz, 1H, 4-H, C_6H_3), 7.52 (d, $^4J_{H,H} = 2.1$ Hz, 1H, 6-H, C_6H_3), 7.58 (br. d, $^3J_{H,H} = 7.9$ Hz, 1H, 4-H, Py), 8.56 (br. s, 3H, arylCHN + 2-H (Py) + 6-H (Py)), 12.76 (s, 1H, OH) ppm. Calc. for $C_{12}H_9BrN_2O$ (277.12): C 52.01, H 3.27; N 10.11. Found: C 51.92, H 3.36, N 10.19.

3. ^{1}H NMR: $\delta = 6.95$ (d, $^3J_{H,H} = 8.8$ Hz, 1H, 3-H, C_6H_3), 7.12 (d. d, $^3J_{H,H} = 4.5$ Hz, $^4J_{H,H} = 1.5$ Hz, 2H, 3-H + 5-H, Py), 7.50 (d. d, $^3J_{H,H} = 8.8$ Hz, $^4J_{H,H} = 2.3$ Hz, 1H, 4-H, C_6H_3), 7.54 (d, $^4J_{H,H} = 2.3$ Hz, 1H, 6-H, C_6H_3), 8.54 (s, 1H, arylCHN), 8.66 (d. d, $^3J_{H,H} = 4.5$ Hz, $^4J_{H,H} = 1.5$ Hz, 2H, 2-H + 6-H, Py), 12.57 (br. s, 1H, OH) ppm. Calc. for $C_{12}H_9BrN_2O$ (277.12): C 52.01, H 3.27; N 10.11. Found: C 52.09, H 3.20, N 10.04.

Single-crystal X-ray diffraction study

X-ray data collection was performed on a Mar345 image plate detector using Mo-K_α radiation (Zr-filter). The data were integrated with the crysAlisPro software.[31] The implemented empirical absorption correction was applied. The structures were solved by direct methods using the SHELXS-97 program[32] and refined by full-matrix least squares on $|F^2|$ using SHELXL-97.[32] Non-hydrogen atoms were anisotropically refined and the hydrogen atoms were placed on calculated positions in riding mode with temperature factors fixed at 1.2 times U_{eq} of the parent atoms. Figures were generated using the program Mercury.[33]

Crystal data for 2. $C_{12}H_9BrN_2O$, $M_r = 277.12$ g mol^{-1}, monoclinic, space group $P2_1/n$, $a = 4.5103(3)$, $b = 19.8005(15)$, $c = 12.1942(8)$ Å, $\beta = 95.592(7)^\circ$, $V = 1083.84(13)$ Å^3, $T = 297(2)$ K, $Z = 4$, $\rho = 1.698$ g cm^{-3}, μ(Mo-Kα) = 3.770 mm^{-1}, reflections: 10 312 collected, 1934 unique, $R_{int} = 0.043$, R_1(all) = 0.0426, wR_2(all) = 0.0979.

Crystal data for 3. $C_{12}H_9BrN_2O$, $M_r = 277.12$ g mol^{-1}, orthorhombic, space group $Pca2_1$, $a = 6.1946(6)$, $b = 7.0152(7)$, $c = 25.100(2)$ Å, $V = 1090.76(17)$ Å^3, $T = 293(2)$ K, $Z = 4$, $\rho = 1.688$ g cm^{-3}, μ(Mo-Kα) = 3.746 mm^{-1}, reflections: 9101 collected, 2076 unique, $R_{int} = 0.047$, R_1(all) = 0.0540, wR_2(all) = 0.1185.

Acknowledgements

This work was funded by the Fonds National de la Recherche Scientifique (FNRS) (PDR T.0102.15) and COST actions MP1202 and CA15128.

References

1 B. Moulton and M. J. Zaworotko, *Chem. Rev.*, 2001, **101**, 1629.
2 (*a*) J. M. Lehn, *Supramolecular Chemistry*, VCH, Weinheim, Germany, 1995; (*b*) L. Brunsveld, B. J. B. Folmer, E. W. Meijer and R. P. Sijbesma, *Chem. Rev.*, 2001, **101**, 4071.
3 G. A. Jeffery, *An Introduction To Hydrogen Bonding*, Oxford University Press, 1997.
4 P. Metrangolo and G. Resnati, *Halogen Bonding: Fundamentals and Applications (Stucture and Bonding)*, Springer, Heidelberg, 2010.
5 G. R. Desiraju, P. S. Ho, L. Kloo, A. C. Legon, R. Marquardt, P. Metrangolo, P. Politzer, G. Resnati and K. Rissanen, *Pure Appl. Chem.*, 2013, **85**, 1711.
6 T. Sakurai, M. Sundaralingam and G. A. Jeffrey, *Acta Crystallogr.*, 1963, **16**, 354.
7 G. R. Desiraju and R. Parthasarathy, *J. Am. Chem. Soc.*, 1989, **111**, 8725.
8 (*a*) P. Metrangolo and G. Resnati, *Chem. Commun.*, 2013, **49**, 1783; (*b*) A. Mukherjee, S. Tothadi and G. R. Desiraju, *Acc. Chem. Res.*, 2014, **47**, 2514; (*c*) G. Cavallo, P. Metrangolo, R. Milani, T. Pilati, A. Priimagi, G. Resnati and G. Terraneo, *Chem. Rev.*, 2016, **116**, 2478.
9 C. B. Aakeröy, M. Fasulo, N. Schultheiss, J. Desper and C. Moore, *J. Am. Chem. Soc.*, 2007, **129**, 13772.
10 P. Metrangolo, G. Resnati, T. Pilati, R. Liantonio and F. J. Meyer, *J. Polym. Sci., Part A: Polym. Chem.*, 2007, **45**, 1.
11 M. Fourmigué and P. Batail, *Chem. Rev.*, 2004, **104**, 5379.
12 (*a*) E. Cariati, G. Cavallo, A. Forni, G. Leem, P. Metrangolo, F. Meyer, T. Pilati, G. Resnati, S. Righetto, G. Terraneo and E. Tordin, *Cryst. Growth Des.*, 2011, **11**, 5642; (*b*) A. Priimagi, G. Cavallo, P. Metrangolo and G. Resnati, *Acc. Chem. Res.*, 2013, **46**, 2686; (*c*) N. Sassirinia, S. Amani, S. J. Teat, O. Roubeau and P. Gamez, *Chem. Commun.*, 2014, **50**, 1003.

13 (*a*) M. Irie, *Chem. Rev.*, 2000, **100**, 1683; (*b*) S. Kobatake and M. Irie, *Annu. Rep. Prog. Chem., Sect. C: Phys. Chem.*, 2003, **99**, 277.

14 (*a*) E. Hadjoudis, M. Vitterakis, I. Moustakali and I. Mavridis, *Tetrahedron*, 1987, **43**, 1345; (*b*) E. Hadjoudis and I. M. Mavridis, *Chem. Soc. Rev.*, 2004, **33**, 579; (*c*) K. Amimoto and T. Kawato, *J. Photochem. Photobiol., C*, 2005, **6**, 207; (*d*) T. Haneda, M. Kawano, T. Kojima and M. Fujita, *Angew. Chem., Int. Ed.*, 2007, **46**, 6643; (*e*) E. Hadjoudis, S. D. Chatziefthimiou and I. M. Mavridis, *Curr. Org. Chem.*, 2009, **13**, 269; (*f*) Y. Inokuma, M. Kawano and M. Fujita, *Nat. Chem.*, 2011, **3**, 349.

15 (*a*) E. Hadjoudis, V. Verganelakis, C. Trapalis and G. Kordas, *Mol. Eng.*, 2000, **8**, 459; (*b*) F. Robert, A. D. Naik, B. Tinant, R. Robiette and Y. Garcia, *Chem.–Eur. J.*, 2009, **15**, 4327; (*c*) F. Robert, A. D. Naik and Y. Garcia, *J. Phys.: Conf. Ser.*, 2010, **217**, 012031; (*d*) Y. Garcia, F. Robert, A. D. Naik, G. Zhou, B. Tinant, K. Robeyns, S. Michotte and L. Piraux, *J. Am. Chem. Soc.*, 2011, **133**, 15850; (*e*) F. Robert, A. D. Naik, B. Tinant and Y. Garcia, *Inorg. Chim. Acta*, 2012, **380**, 104.

16 P.-L. Jacquemin, Y. Garcia and M. Devillers, *J. Mater. Chem. C*, 2014, **2**, 1815.

17 (*a*) F. Robert, A. D. Naik, F. Hidara, B. Tinant, R. Robiette, J. Wouters and Y. Garcia, *Eur. J. Org. Chem.*, 2010, 621; (*b*) F. Robert, P.-L. Jacquemin, B. Tinant and Y. Garcia, *CrystEngComm*, 2012, **14**, 4396; (*c*) D. A. Safin, K. Robeyns and Y. Garcia, *CrystEngComm*, 2012, **14**, 5523; (*d*) D. A. Safin, K. Robeyns and Y. Garcia, *RSC Adv.*, 2012, **2**, 11379; (*e*) P.-L. Jacquemin, K. Robeyns, M. Devillers and Y. Garcia, *Chem. Commun.*, 2014, **50**, 649; (*f*) P.-L. Jacquemin, K. Robeyns, M. Devillers and Y. Garcia, *Chem.–Eur. J.*, 2015, **21**, 6832; (*g*) D. A. Safin, K. Robeyns, M. G. Babashkina, Y. Filinchuk, A. Rotaru, C. Jureschi, M. P. Mitoraj, J. Hooper, M. Brelac and Y. Garcia, *CrystEngComm*, 2016, DOI: 10.1039/c6ce00266h.

18 (*a*) R. Custelcean and J. E. Jackson, *Chem. Rev.*, 2001, **101**, 1963; (*b*) C. Schalley, *Introduction in Analytical Methods in Supramolecular Chemistry*, ed. C. Schalley, WILEY-VCH Verlag GmbH & Co. KGaA, Weinheim, 2007, pp. 1–16.

19 (*a*) I. Moustakali-Mavridis, E. Hadjoudis and A. Mavridis, *Acta Crystallogr.*, 1978, **34**, 3709; (*b*) A. M. Atria, M. T. Garland, E. Spodine and L. Toupet, *Acta Crystallogr., Sect. A: Found. Crystallogr.*, 1991, **47**, 1116.

20 M. A. Spackman and D. Jayatilaka, *CrystEngComm*, 2009, **11**, 19.

21 M. A. Spackman and J. J. McKinnon, *CrystEngComm*, 2002, **4**, 378.

22 S. K. Wolff, D. J. Grimwood, J. J. McKinnon, M. J. Turner, D. Jayatilaka and M. A. Spackman, *CrystalExplorer 3.1*, University of Western Australia, 2012.

23 C. Jelsch, K. Ejsmont and L. Huder, *IUCrJ*, 2014, **1**, 119.

24 A. Bondi, *J. Phys. Chem.*, 1964, **68**, 441.

25 (*a*) D. A. Safin, M. Bolte and Y. Garcia, *CrystEngComm*, 2014, **16**, 5524; (*b*) D. A. Safin, M. Bolte and Y. Garcia, *CrystEngComm*, 2014, **16**, 8786.

26 D. A. Safin, K. Robeyns and Y. Garcia, *CrystEngComm*, 2012, **14**, 5523.

27 J. Harada, T. Fujiwara and K. Ogawa, *J. Am. Chem. Soc.*, 2007, **129**, 16216.

28 M. Sliwa, S. Létard, I. Malfant, M. Nierlich, P. G. Lacroix, T. Asahi, H. Masuhara, P. Yu and K. Nakatani, *Chem. Mater.*, 2005, **17**, 4727.

29 (*a*) M. D. Cohen and G. M. J. Schmidt, *J. Phys. Chem.*, 1962, **66**, 2442; (*b*) M. D. Cohen, G. M. J. Schmidt and S. Flavian, *J. Chem. Soc.*, 1964, 2041; (*c*) M. D. Cohen, Y. Hirshberg and G. M. J. Schmidt, *J. Chem. Soc.*, 1964, 2051; (*d*) M. D. Cohen, Y. Hirshberg and G. M. J. Schmidt, *J. Chem. Soc.*, 1964, 2060; (*e*) J. Bregman, L. Leiserowitz and G. M. J. Schmidt, *J. Chem. Soc.*, 1964, 2068; (*f*) M. D. Cohen and S. Flavian, *J. Chem. Soc. B*, 1967, 317; (*g*) M. D. Cohen and S. Flavian, *J. Chem. Soc. B*, 1967, 321; (*h*) M. D. Cohen, S. Flavian and L. Leiserowitz, *J. Chem. Soc. B*, 1967, 329; (*i*) M. D. Cohen and S. Flavian, *J. Chem. Soc. B*, 1967, 334; (*j*) M. D. Cohen, *J. Chem. Soc. B*, 1968, 373.

30 M. S. M. Rawat, S. Mal and P. Singh, *Open Chem.*, 2015, **2**, 7.

31 *Rigaku Oxford Diffraction, CrysAlis(Pro) Software system, version 1.171.36.21*, Rigaku Corporation, Oxford, UK, 2012.

32 G. M. Sheldrick, *Acta Crystallogr., Sect. A: Found. Crystallogr.*, 2008, **64**, 112.

33 I. J. Bruno, J. C. Cole, P. R. Edgington, M. Kessler, C. F. Macrae, P. McCabe, J. Pearson and R. Taylor, *Acta Crystallogr., Sect. A: Found. Crystallogr.*, 2002, **58**, 389.

